A Numerical Study of ICA for Separating Monopole, Dipole, and Quadrupole Acoustic Sources

Hajer HAMDAOUI
Laboratory of Mechanics, Modeling and Productivity (LA2MP), National School of Engineers of Sfax, University of Sfax, BP N ° 1173 - 3038, Sfax, Tunisia, Faculty of Science of Sfax, University of Sfax, BP n ° 1171 - 3000 Sfax, hajer.hamdaoui33@gmail.com

Dhouha TOUNSI
Laboratory of Mechanics, Modeling and Productivity (LA2MP), National School of Engineers of Sfax, University of Sfax, BP N ° 1173 - 3038, Sfax, Tunisia, dhouha.ing@gmail.com

Mohamed TAKTAK*
Laboratory of Mechanics, Modeling and Productivity (LA2MP), National School of Engineers of Sfax, University of Sfax, BP N ° 1173 - 3038, Sfax, Tunisia, Faculty of Science of Sfax, University of Sfax, BP n ° 1171 - 3000 Sfax, Mohamed.taktak@fss.rnu.tn; Mohamed.taktak.tn@gmail.com

Mohamed HADDAR
Laboratory of Mechanics, Modeling and Productivity (LA2MP), National School of Engineers of Sfax, University of Sfax, BP N ° 1173 - 3038, Sfax, Tunisia, mohamed.haddar@enis.tn

* Author to whom correspondence should be addressed

Abstract: - This paper presents a simulation-based study on the application of Independent Component Analysis (ICA) for separating idealized acoustic sources modeled as monopoles, dipoles, and quadrupoles. The work focuses on evaluating ICA performance in controlled synthetic configurations rather than experimental or real-world scenarios. Analytical models are used to generate pressure and particle-velocity fields for different multipole arrangements, which serve as input signals to the FastICA algorithm. Simulations include dipole cases (in-phase and anti-phase) and quadrupole configurations (lateral and longitudinal). Results show that ICA can recover the temporal structure and frequency content of the sources, despite the inherent amplitude-scaling ambiguities of the method. This study provides a preliminary assessment of ICA's capabilities in simplified acoustic environments and highlights its potential for future applications in noise analysis and source separation.

Keywords: FASTICA, source identification, BSS, pulsating sphere, monopole, dipole and quadrupole sources

1. INTRODUCTION

In engineering acoustics and structural dynamics, sound and vibration arise from the same core mechanisms: source generation, wave propagation (with dispersion, attenuation, and reflections), and radiation whose directivity depends on source order and geometry. Reliable prediction and control, therefore, require time-frequency-faithful excitations and dynamic analyses, as static proxies can be inadequate for vibration-controlled systems [1]. Moreover, the selection/scaling of input records governs response dispersion, and the combined effects of duration, intensity, and magnitude shape structural stability that directly motivate using multipole source models and FastICA to disentangle mixed acoustic fields [2–3].

In industrial machinery and environments, a wide variety of noise sources can be identified, including rotors, stators, gears, fans, vibrating panels, turbulent fluid flows, impact processes, electric machines, and internal combustion engines [4]. These sources contribute significantly to the overall acoustic environment in factories and workshops.

In fact, understanding the nature of sound sources is essential for accurate modeling and effective noise control. Sound sources are typically classified into

three fundamental types based on their radiation characteristics: monopoles, dipoles, and quadrupoles [5, 6].

A monopole is the simplest form of acoustic source. It radiates sound equally in all directions and is often modeled as a small pulsating sphere that expands and contracts uniformly [6]. In fact, Several studies have investigated the characteristics and applications of acoustic monopoles. Russell, Titlow, and Bemmen [7] provided an experimental demonstration of monopole radiation patterns using loudspeaker arrays, highlighting their omnidirectional nature compared to dipoles and quadrupoles. Ochmann [8] developed exact analytical solutions for sound radiation from a moving monopole above an impedance plane, accounting for Doppler effects and reflections. Kayser, Dragna, and Blanc-Benon [9] proposed a heuristic model for monopole radiation in a moving and inhomogeneous atmosphere, validated through 3D simulations, with applications to aircraft noise prediction. Moruzzi, Cinefra, and Bagassi [10] implemented a monopole source in a finite-element framework (CUF) to analyze vibro-acoustic behavior in closed cavities, demonstrating its relevance for transmission loss estimation. Additionally, Duan and Kirby [11] examined the sound power output of a monopole in cylindrical ducts with area discontinuities, revealing modal interactions and reflection effects. These works collectively emphasize the monopole's role as a fundamental acoustic source and its importance in theoretical, experimental, and computational acoustics.

A dipole consists of two closely spaced monopoles of equal strength but opposite phase. While one source expands, the other contracts, resulting in a back-and-forth motion of the surrounding fluid. Dipole sources are commonly found in vibrating structures or unbaffled loudspeakers [6, 7]. Recent research continues to explore their unique properties:

Zhan et al [12] introduced a dipole surface source structure designed for low-frequency noise reduction in vibrating equipment. By arranging concentric pistons in opposite phase and optimizing amplitude and area ratios, they demonstrated effective attenuation through destructive interference.

Eastland, Curry & Tolliver [13] investigated helical wave generation using orthogonal dipoles. Their experimental and numerical work shows how phase-shifted dipole arrangements can control wavefront shape and directionality in specific acoustic applications.

Martischang, Roux & Baudoin [14] analyzed the phenomenon of a dipole "surfing" its own acoustic field, revealing a self-induced radiation force aligned with the motion. This wave–particle-style interaction highlights novel dynamics of dipole sources in fluid media.

A quadrupole is formed by combining two dipoles in opposite phase. It can be arranged in different configurations, such as lateral (dipoles placed perpendicularly) or longitudinal (dipoles aligned along the same axis). These sources are typically associated with turbulent flows, such as those found in jet engines or high-speed fans, and are less efficient radiators of low-frequency sound compared to monopoles and dipoles [8]. Kopiev et al. [15] developed a low-order quadrupole model for turbulent jet noise based on Lighthill's acoustic analogy and validated it via multi-microphone measurements. They identified the spatial zones where quadrupole emission dominates and demonstrated its importance in predicting both near-field and far-field jet noise spectra. Brentner [16] provided exact calculations of quadrupole contributions for incompressible flows, emphasizing that neglecting quadrupole terms can significantly underestimate the acoustic pressure, particularly for propeller and rotor noise. Kojima et al. [17] investigated quadrupole noise from the trailing edge of a NACA0012 airfoil using vortex-sound theory and dynamic mode decomposition, finding that vortex shedding interactions lead to high-frequency quadrupole radiation under higher Mach conditions. These elementary source models are fundamental to the theoretical and numerical analysis of sound radiation. They serve as building blocks for more complex source configurations and are widely used in the development of source separation algorithms, such as Independent Component Analysis (ICA), which aims to isolate individual sources from mixed acoustic signals.

In real-world applications, the signals captured by these sensors are typically mixtures of multiple source signals. The task of source separation involves estimating the original source signals from these observed mixtures, a problem addressed by Blind Source Separation (BSS) techniques. The concept of Blind Source Separation emerged in the mid-1980s with the seminal work of Hérault, Jutten, and Ans [18] who introduced a neuromimetic architecture capable of separating mixed signals through unsupervised learning. Building on this foundation, Jutten and Hérault [19] proposed an adaptive algorithm based on local learning rules, marking the first formal approach to BSS. In 1994, Comon established the theoretical framework of Independent Component Analysis (ICA), defining statistical independence as the key criterion for source separation. Shortly after, Bell and Sejnowski

[20] introduced the InfoMax algorithm, which leverages information theory to maximize entropy in ICA. The late 1990s saw significant progress with Hyvärinen's FastICA algorithm [21], offering a fast and robust fixed-point method for ICA. This evolution culminated in comprehensive treatments such as Hyvärinen, Karhunen, and Oja's book [22], which consolidated ICA theory and applications, and later the Handbook of Blind Source Separation by Comon and Jutten [23], summarizing decades of research. More recent surveys, including Mansour et al. [24] and Sawada et al. [25], have expanded the scope of BSS to modern contexts, integrating ICA with techniques like Nonnegative Matrix Factorization for audio and speech processing.

BSS is particularly valuable in scenarios where the mixing process is unknown. Over the past three decades, BSS has evolved into a major research area in signal processing, with applications ranging from speech enhancement and mechanical machine diagnosis to acoustic imaging and underwater acoustics. In fact, Li. D et al [26] addressed the challenge of separating underwater acoustic signals from a single-channel mixture. The authors propose an improved algorithm combining Non-negative Matrix Factorization (NMF) and Fast Independent Component Analysis (FastICA). The method enhances separation accuracy and robustness in noisy underwater environments, outperforming traditional ICA-based approaches in terms of signal-to-interference ratio and computational efficiency. Indeed, the study of Al-Qaisi.A [27] improves the Fast ICA algorithm for blind source separation of mixed audio signals under noisy conditions. The enhancement focuses on optimizing convergence speed and stability by introducing adaptive learning rates and pre-processing steps. Experimental results show significant improvements in separating speech and music signals compared to standard FastICA.

Two consecutive studies by the same research team focused on fault diagnosis in spur gear transmissions using advanced signal processing techniques. Taktak et al. [28] applied the Independent Component Analysis (ICA) method to vibration signals from a one-stage spur gear transmission crankcase. By decomposing the signals into statistically independent components, they successfully isolated fault-related features, improving detection accuracy and reducing interference from other mechanical sources. Building on this work, Akrout et al. [29] introduced an inverse method combined with ICA to reconstruct source signals from measured vibrations. This approach enabled more precise identification of gear defects and demonstrated superior diagnostic reliability compared to direct signal analysis, particularly under complex operating conditions. Together, these studies highlight the evolution from component separation to inverse modeling, offering a robust framework for gear fault diagnosis in automotive and industrial applications.

Recent advances have highlighted the growing synergy between blind source separation techniques such as FastICA and modern machine learning approaches. Wu et al. (2025) demonstrated that incorporating deep learning into acoustic imaging significantly enhances the separation of incoherent sources, addressing limitations of traditional ICA-based methods in complex environments [30].

This study addresses the separation of acoustic signals generated by a dipole and a quadrupole (both longitudinal and lateral) using the FastICA algorithm. The work combines blind source separation with detailed modeling of the acoustic field, including the determination of key physical quantities, such as sound pressure and particle velocity, for each source type. By applying FastICA to mixed measurements (velocities), the method successfully isolates individual contributions from multipole sources, demonstrating its effectiveness in complex acoustic environments and its potential for advanced noise-source identification.

The paper is organized as follows. The studied problem and the multipole acoustic source models are presented in Section 2. Section 3 then provides a detailed presentation of the fundamentals of the FASTICA algorithm. Finally, numerical results are presented and discussed in Section 4.

2. FUNDAMENTAL CONCEPTS OF ACOUSTIC MULTIPOLES

The purpose of this section is to introduce the fundamental concepts related to acoustic multipoles. As their name implies, these sources (monopoles, dipoles, and quadrupoles) exhibit relatively simple radiation patterns and properties, which allow them to be described analytically using mathematical models. This analytical tractability makes multipoles highly valuable in acoustics for approximating the behavior of real, complex sources. For instance, the complex radiation field produced by an extended source, such as a vibrating panel or a loudspeaker array, can often be effectively represented as a superposition of multiple monopoles and higher-order multipoles.

In this work, we focus specifically on three types of sources: Monopoles, Dipoles, and Quadrupoles.

By restricting our study to these three fundamental source types, we can leverage their well-understood analytical properties to model and analyze more intricate acoustic phenomena.

2.1. Acoustic monopole definition and radiation

An acoustic monopole is a point source that radiates omnidirectional, divergent spherical waves. In practical terms, a monopole can be modeled as a small pulsating sphere with a radius (r_s) much smaller than the wavelength of the emitted sound. This idealization allows for analytical treatment of its radiation properties.

The monopole's radiation is characterized by its volumetric velocity through a spherical surface of radius (r_s):

$$Q = V.S = 4\pi r_s^2 V \tag{1}$$

where: Q is the volume velocity, V is the normal velocity of the sphere's surface, and S is the surface area of the sphere.

In the far field, the acoustic pressure at a distance (r) from the source can be expressed as:

$$P = \frac{i\omega\rho Q}{4\pi r} e^{i(\omega t - k_0 r)} \tag{2}$$

where: P is the acoustic pressure, ω is the angular frequency, ρ is the density of the medium, k_0 is the wave number, and t is time.

According to Euler's equation, the radial component of the acoustic particle velocity is given by equation (3):

$$u(r,t) = \frac{Q}{4\pi}\left(\frac{1}{r^2} + \frac{ik_0}{r}\right)\left(\cos(\omega t - k_0 r)\right) \tag{3}$$

This analytical framework provides a foundation for understanding more complex source types, such as dipoles and quadrupoles.

2.2. An acoustic dipole

An **acoustic dipole** is a fundamental point source in acoustics, constructed from two closely spaced monopoles of equal strength. They can be in phase or opposite phase. While a monopole radiates sound equally in all directions, a dipole's configuration causes it to radiate with a characteristic figure-eight directivity pattern. The dipole can be visualized as two pulsating spheres: one expanding while the other contracts, separated by a small distance. Dipoles are commonly used in acoustics to model vibrating structures or unbaffled loudspeakers, as they represent a sound source composed of two monopoles of opposite strength separated by a small distance. This model effectively describes the distinctive directivity of systems that generate sound fields with regions of positive and negative pressure, such as vibrating membranes or tuning forks. Møller and Juhl explain that the sound radiation of a dipole strongly depends on the frequency and geometry of the source, making it an essential tool for studying complex acoustic systems [31].

Pelat emphasizes that elementary acoustic fields, including the dipole, are fundamental for understanding wave propagation and interaction in various media [32]. Finally, Russel (2000) illustrates the practical application of this concept by analyzing the sound field emitted by a tuning fork, which behaves as a typical acoustic dipole with marked directivity and a rapid decrease in sound intensity with distance [33].

2.2.1. Interaction of two-point sources in phase

Now, we are interested in the acoustic field radiated by two-point sources separated by a distance 2d, oscillating with flow rates:

$$\begin{aligned} Q_1(t) &= \dot{Q}_1 e^{-i\omega t} \\ Q_2(t) &= \dot{Q}_2 e^{-i\omega t} \end{aligned} \tag{4}$$

with $Q_1(t) = Q_2(t) = Q(t)$ (5)

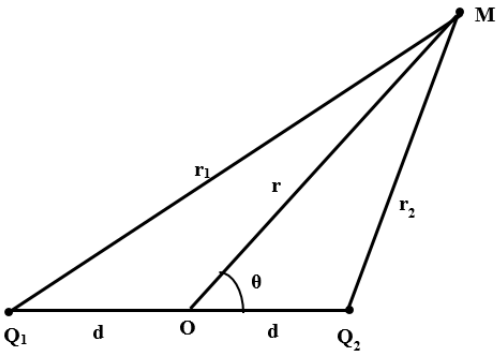

Figure 1. Representation of two sources separated by a distance 2d

The total acoustic pressure at a field point r and time t is given by the superposition of the pressures radiated by each monopole:

$$P(r_1,r_2,t) = \frac{i\omega\rho}{4\pi}\left[\frac{Q_1 e^{i(\omega t - k_0 r_1)}}{r_1} + \frac{Q_2 e^{i(\omega t - k_0 r_2)}}{r_2}\right] \tag{6}$$

where: r_1 and r_2 are the positions of two sources. Q_1 and Q_2 are their respective volume flow rates. So, taking into account equation .2 we find:

$$P(r_1,r_2,t) = \frac{i\omega\rho Q}{4\pi}\left[\frac{e^{i(\omega t - k_0 r_1)}}{r_1} + \frac{e^{i(\omega t - k_0 r_2)}}{r_2}\right] \tag{7}$$

According to figure.1, the vectors r_1 and r_2 have the respective expressions:

$$r_1 = \begin{pmatrix} r\cos\theta + d \\ r\sin\theta \end{pmatrix} \quad et \quad r_2 = \begin{pmatrix} r\sin\theta - d \\ r\sin\theta \end{pmatrix} \tag{8}$$

So:

$$\left\{\begin{matrix} |r_1| = \sqrt{r^2 + d^2 + 2dr\,cos\theta} \\ |r_2| = \sqrt{r^2 + d^2 - 2dr\,cos\theta} \end{matrix}\right\} \tag{9}$$

The pressure field resulting from the radiation of two sources in phase with the acoustic flow rates of each being equal, therefore has the expression [31]:

$$p(r,\theta)=\frac{\rho\dot{Q}}{4\pi}\left[\frac{\exp(-ik_0\sqrt{r^2+d^2+2dr\cos(\theta)})}{\sqrt{r^2+d^2+2dr\cos(\theta)}}+\frac{\exp(-ik\sqrt{r^2+d^2-2dr\cos(\theta)})}{\sqrt{r^2+d^2-2dr\cos(\theta)}}\right] \quad (10)$$

In the far field ($d>>r$), we can approximate:

$$r_1^2=r^2(1+\frac{2d\cos(\theta)}{r})\rightarrow r_1\simeq r(1+\frac{d\cos(\theta)}{r})=r+d\cos(\theta) \quad (11)$$
$$r_2^2=r^2(1-\frac{2d\cos(\theta)}{r})\rightarrow r_2\simeq r(1-\frac{d\cos(\theta)}{r})=r-d\cos(\theta)$$

So, the pressure will have the following expression:

$$p(r,\theta)=\frac{\rho_0\dot{q}}{4\pi r}\exp(-ikr)\cos(kd\cos(\theta)) \quad (12)$$

The wavelength is greater than the distance d, i.e., if $k_0d << 1$, then the sound pressure can be put in the form:

$$p(r)=\frac{i\omega\rho_0 q_0}{4\pi r}\exp(-ikr) \quad (13)$$

In the far field, the radiation from two point sources in phase is therefore isotropic and

The amplitude of the radiated pressure is equal to the acoustic pressure radiated by a single point source of double flow.

The radial velocity is then equal to the radiated velocity of a single point source of double flow, and it is expressed as follows:

$$U(r,\theta)=\frac{Q}{4\pi}(\frac{1}{r^2}+\frac{ik_0}{r})\exp(\omega t-ik_0r)\cos(k_0d\cos(\theta)) \quad (14)$$

2.2.2. Interaction of two-point sources antiphase

When the two sources are in phase opposition, their volume flow rates are equal in magnitude but opposite in sign:

$$Q_1(t)=-Q_2(t)=Q(t) \quad (15)$$

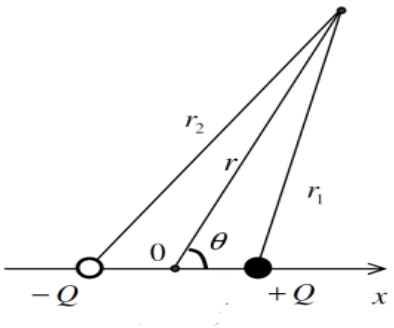

Figure 2. Representation of two-point sources in antiphase [31]

The pressure field resulting from the radiation from these two sources is therefore the sum of the pressure fields created by each of the sources:

$$p(r,\theta)=\frac{\rho\dot{Q}}{4\pi}\left[\frac{\exp(-ik_0\sqrt{r^2+d^2+2dr\cos(\theta)})}{\sqrt{r^2+d^2+2dr\cos(\theta)}}-\frac{\exp(-ik_0\sqrt{r^2+d^2-2dr\cos(\theta)})}{\sqrt{r^2+d^2-2dr\cos(\theta)}}\right] \quad (16)$$

In the far fields, the pressure equation is:

$$P(r,t)=\frac{i\omega\rho Q}{4\pi r}\left(ik_0d\cos(\theta)\right)e^{i(\omega t-k_0r)} \quad (17)$$

The radiation from two point sources in antiphase is not isotropic but presents a few directions.

The acoustic particle radial velocity has the expression [31]:

$$u(r,t)=\frac{Q}{4\pi}\left(\frac{1}{r^2}+\frac{ik_0}{r}\right)\left(ik_0d\cos\theta\right)e^{i(\omega t-k_0r)} \quad (18)$$

2.3. An acoustic quadrupole

Quadrupole sources play a fundamental role in acoustics, as they represent a higher-order configuration of sound radiation compared to monopoles and dipoles. A quadrupole consists of two dipoles arranged in such a way that their combined radiation pattern exhibits even greater directivity and a faster decay of sound intensity with distance. Classic examples of quadrupole behavior include the tuning fork and the wine glass. The tuning fork, as analyzed by Russel, radiates sound primarily through its vibrating prongs, which act as two opposing dipoles; their interaction creates a quadrupole-like field with minimal energy radiated along the axis of vibration [32]. Similarly, the wine glass produces sound when its rim vibrates in complex modes, generating alternating regions of compression and rarefaction that resemble a quadrupole source, as discussed in studies on elementary acoustic fields (Pelat, 2020) [32]. These configurations are essential for understanding the radiation characteristics of musical instruments and resonant structures, where symmetry and vibration modes significantly influence the acoustic field.

There are two configurations:

- **Lateral configuration:** The four sources are positioned at the corners of a square with side length (2d) (**Figure 3**), and their oscillations are arranged such that each source is out of phase with its neighbors. This setup creates a two-dimensional quadrupole pattern, often used to model sources with complex directivity.

- **Longitudinal configuration:** The four sources are aligned along a straight line (**Figure 3),** each separated by a distance (2d). In this case, the two outer sources oscillate in antiphase with the two inner sources. This arrangement produces a quadrupole field with a different spatial distribution, relevant for modeling elongated vibrating structures. These idealized configurations allow for analytical modeling of quadrupole radiation and provide insight into the behavior of more complex acoustic sources.

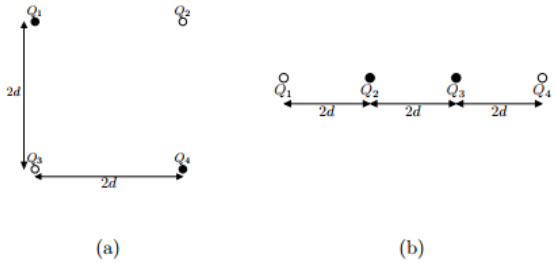

Figure 3. Schematics of the two arrangements: (a) four square sources and (b) four aligned sources. [31]

2.3.1. Lateral quadrupole configuration

Four point sources are placed at the corners of a square of side 2d. The sources phase shifted such that each is out of phase with its neighbor, creating a two-dimensional quadrupole. The total far-field pressure is expressed as follows [31]:

$$P(r,t)=\frac{1}{2}\frac{\rho\dot{Q}}{4\pi}(k_0 d)^2\sin(2\theta)e^{i(\omega t-k_0 r)} \quad (19)$$

The radial component of the acoustic particle velocity has the expression [28]:

$$u(r,t)=\frac{1}{2}\frac{Q}{4\pi}\left(\frac{1}{r^2}+\frac{ik_0}{r}\right)(k_0 d)^2\sin(2\theta)e^{i(\omega t-k_0 r)} \quad (20)$$

2.3.2. Longitudinal quadrupole configuration

Four-point sources are aligned along a straight line, each separated by 2d. The two outer are in antiphase with the two inner sources. The far field pressure has the following expression:

$$p(r,t)=2\frac{\rho\dot{Q}}{4\pi r}(k_0 d)^2(\cos\theta)^2 e^{i(\omega t-k_0 r)} \quad (21)$$

The radial component of the acoustic particle velocity has the expression:

$$u(r,t)=2\frac{Q}{4\pi}\left(\frac{1}{r^2}+\frac{ik_0}{r}\right)(k_0 d)^2 e^{i(\omega t-k_0 r)} \quad (22)$$

$$u(r,t)=\frac{1}{2}\frac{Q}{4\pi}\left(\frac{1}{r^2}+\frac{ik_0}{r}\right)(k_0 d)^2\sin(2\theta)e^{i(\omega t-k_0 r)} \quad (23)$$

3. THEORY AND IMPLEMENTATION OF ICA/FASTICA

3.1. ICA concept

ICA is a statistical method that processes vector (multivariate) observations to extract linear components that are as independent as possible. This simple idea has proven very successful for signal processing. More generally, it is used in all cases where a system of multiple sensors, providing coherent signals (or images), is listening to a discrete set of sources that we seek to extract from the observations and that we can, for physical reasons, assume to be mutually statistically independent [34].

The ICA method considered in this paper is a linear mixture formulated as follows:

$$\{X\}=[A]\{S\} \quad (23)$$

In matrix form:

$$\{X(t)\}=[A]\{S(t)\}+\{b(t)\} \quad (24)$$

where:

$X(t)=[X_1(t),\ldots\ldots,X_M(t)]^T$: is the vector of M observations.

$S(t)=[S_1(t),\ldots\ldots,S_N(t)]^T$: is the vector of the N source signals ($M \geq N$).

$[A]$ is the mixing matrix of size $M\times N$ (unknown), and *b(t)* is a possible additive noise.

We recall that the only hypothesis on the sources is their statistical independence.

In order to apply for ICA correctly, a necessary condition must be met: the number of sources must be less than or equal to the number of observations.

The goal of the ICA method is to estimate the unmixing matrix W ($[W]=[A]^{-1}$)such that:

$$Y(t)=W.X(t) \quad (25)$$

with components as independent as possible.

Independent Component Analysis (ICA) is a statistical method for blind source separation that seeks to recover original source signals from observed mixtures by exploiting their statistical independence.

The components of the random variable $X(t)=[X_1(t),\ldots\ldots,X_M(t)]^T$are said to be mutually independent statistically if and only if:

$$P(X)=\prod_{i=1}^{M}P(x_i) \quad (26)$$

where *P(X)* is the distribution of X and $\prod_{i=1}^{M}P(x_i)$ is the product of its marginal distributions.

ICA assumes a linear mixing model and aims to minimize mutual dependence between components while maximizing non-Gaussianity, which serves as a measure of independence (Comon, 1994; Hyvärinen & Oja, 2000) [34,35]. The method relies on preprocessing steps such as centering and whitening.

3.2 Preprocessing steps:

Before applying ICA, the observed signals were preprocessed as follows:

- **Centering:** Each observation was centered by subtracting its mean to ensure a zero mean.

$$X_{centered} = x - E(x) \quad (27)$$

- **Whitening:** Principal Component Analysis (PCA) was used to decorrelate the data and normalize variances. Whitening improves convergence and numerical stability.

Originally, the mixing matrix A contains n^2 elements, which represent the parameters to be determined. However, after whitening the data, the problem is simplified because the mixing matrix is restricted to being an orthogonal matrix. An orthogonal matrix has only $\frac{n(n-1)}{2}$ degrees of freedom instead of n^2 for a general matrix.

3.3. FastICA algorithm

The primary objective of Fast ICA is to extract independent components from mixtures of signals by maximizing their non-Gaussianity. FastICA employs higher-order statistics to identify statistically independent signals [35][36].

It is based on the principle of the fixed-point iterative learning algorithm. (Fixed point algorithm).

The network learning algorithm seeks to find a direction that is actually a vector w such that the projection $w^T x$ maximizes the non-Gaussian aspect. To do this, the algorithm uses the fixed-point theorem.

To prevent the vectors from converging to the same maximum, we must decorrelate the projections $w_1^T x, w_2^T x, \ldots\ldots, w_n^T x$ after each iteration.

FastICA's algorithm can be reformulated as a negentropy contrast function.

In fact, Negentropy can be calculated using higher order cumulants, which are defined by Jones and Sibson [37] as:

$$J(y) \approx \frac{1}{12} E\{y^3\}^2 + \frac{1}{48} Kurt(y)^2 \quad (28)$$

This approximation is not robust, which is why Hyvarinen [6] generally uses an approximation defined from a non-quadratic function G such that:

$$neg(y(n)) \approx \left(E\left\{G\left(y_{gauss}(n)\right)\right\} - E\{G(y(n))\}\right)^2 \quad (29)$$

The strength of this approximation is the choice of G; the researchers' work has shown that the best functions used are given by:

$$G(u) = \log\cos hu \quad (30)$$

This choice is robust for both sub-Gaussian and Super-Gaussian sources.

3.4. Algorithm Steps:

The FastICA algorithm begins by taking the preprocessed observation matrix, which has been centered and whitened to ensure zero mean and decorrelated data. For each component, the method applies a fixed-point iteration based on a chosen non-linear function to maximize non-Gaussianity. After each update, the weight vector is normalized to maintain unit length, and an orthogonalization step using the Gram–Schmidt procedure is performed to preserve independence among components.

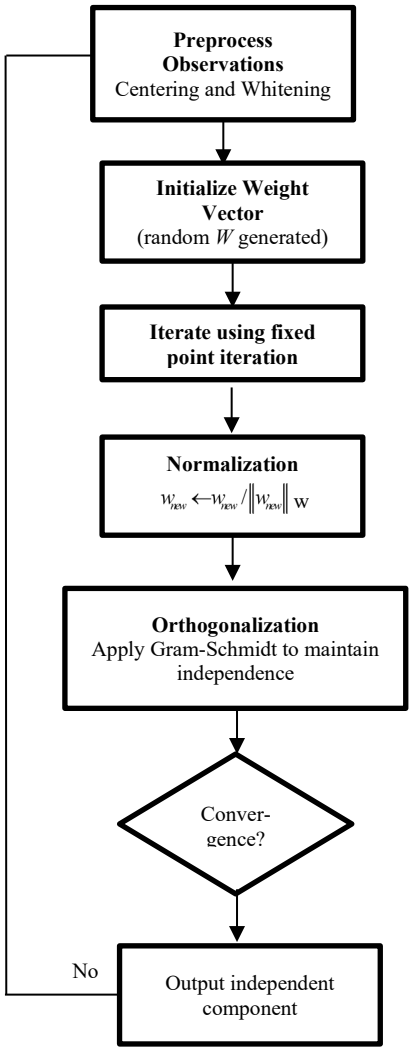

Figure 4. FASTICA Steps

These steps are repeated until convergence, which is verified by monitoring changes in the weight vectors against a predefined threshold or maximum iteration limit. The final output consists of the estimated independent components, which correspond to the original sources up to scaling and permutation indeterminacies (an inherent property of ICA). To address these ambiguities, the analysis focuses on comparing waveform shapes and frequency content rather than absolute amplitude**.**

4. SIMULATION RESULTS

To validate the proposed method, the physical properties of the studied wave are presented in Table 1. The mechanical and geometric properties of the sensors are presented in Table 2.

Table1. Physical properties of the studied waves

Velocity at r=a « V_0»	0.5m/s
Pulsation «ω»	$2.10^3\pi$ rad
Density « ρ_0 »	1,2 kg/m^3
Celerity « c »	340m/s
Wave number « k »	ω/c rad/m

Table 2. Mechanical and geometric properties of the sensors

The 1^{st} *sensor dimensions*	
Source radius « a »	0,009m
Distance between the center and the sensor « r »	2m
Distance between the center and the source « d »	0,05m
Angle between r and d « θ »	$\frac{\pi}{4}$
The 2^{nd} sensor dimensions	
Source radius « a »	0.009m
Distance between the center and the sensor « r »	5m
Distance between the center and the source « d »	0,05m
Angle between r and d « θ »	$\frac{\pi}{6}$

4.1. Assumptions and Physical Regime

The multipole models adopted in this study are based on standard acoustic assumptions:

- **Small source approximation:** Each monopole is modeled as a pulsating sphere with radius a≪λ. For our case, a=0.009 m and λ≈0.34 m (for f≈1000), giving ka≈0.17≪1, which satisfies the monopole condition.
- **Far-field approximation:** Analytical expressions for pressure and velocity assume kr≫1. For r=2 m and k≈18.5 rad/m, we have kr≈37≫1, validating the far-field assumption.
- **Linear acoustics:** The oscillation amplitude is small (V_0=0.5 m/ s), ensuring that acoustic perturbations remain in the linear regime.
- **Frequency range:** The chosen pulsation (ω=2×10^3π rad/s, i.e., f≈1000 Hz) corresponds to audible frequencies where multipole approximations are widely applied.
- **Spacing condition:** For dipoles and quadrupoles, the separation d=0.05 satisfies k0d≪1 (k0d≈0.93), which is acceptable for low-order multipole modeling.

These conditions are consistent with experimental setups reported by Russell et al. (1999) [7] and other references, ensuring that the parameters in Tables 1–2 are physically meaningful and representative of practical acoustic applications.

In order to extract the estimated sources, the observed signals (velocities) are determined and used as input to the ICA algorithm.

4.2. Parameters of the algorithm

-**Initialization:** Weight vectors were initialized randomly with unit norm.
-**Number of components:** Equal to the number of sources (two for dipole, four for quadrupole).
-**Stopping criterion:** Iterations stopped when the change in weight vectors was below 10^{-6}or after a maximum of 500 iterations.
-**Convergence check:** Orthogonalization was applied after each iteration to prevent multiple components from converging to the same solution. Convergence was verified by monitoring the norm difference between successive weight vectors.

4.3. Simulation Framework and Data generation

The synthetic “measured” velocities used as ICA inputs were computed from the analytical expressions of acoustic pressure and particle velocity for monopole, dipole, and quadrupole sources. The simulation was carried out under the following conditions:
-**Time discretization and sampling**: The signals were sampled at a frequency of fs=10 kHz, which is more than 10 times the highest source frequency (f≈1 kHz) to satisfy the Nyquist criterion.
-**Simulation duration:** Each signal was generated over T=1 s, resulting in N=10,000 time samples per observation.

-**Analytical computation**: At each time step, the instantaneous particle velocity was calculated using the far-field expressions derived in Section 2 for the corresponding source configuration.
-**Observation points**: Velocities were computed at two sensor positions for dipole cases and four positions for quadrupole cases, as specified in Table 2.
-**Noise model:** To emulate realistic conditions, additive Gaussian noise with a signal-to-noise ratio (SNR) of 40 dB was introduced to the simulated measurements.
-**Normalization:** Before applying ICA, the signals were centered and whitened as part of the preprocessing step described in Section 3.

This setup ensures that the generated data accurately reflects the theoretical acoustic fields while providing sufficient temporal resolution for ICA processing. The choice of sampling frequency, duration, and SNR is consistent with standard practices in acoustic signal analysis and guarantees reproducibility.

4.4. Results of acoustic dipole configuration

In this context, two configurations are considered: sources oscillating in phase and sources oscillating in antiphase. To determine the velocity of each source, measurements are taken at two distinct points, where sound level meters are positioned to capture the velocity associated with each source (Figures 4 and Figure 6).

4.4.1. Sources in phase

These measured velocities serve as inputs to the source separation algorithm, which is then used to identify the acoustic pressure contribution from each individual source presented in Figure 5 and Figure 7.

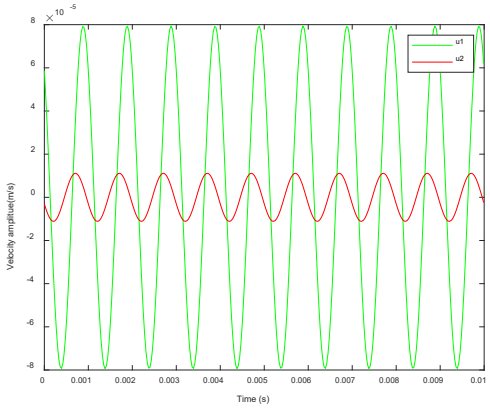

Figure 4. Velocities of each source

For the case of two-phased sources, the resulting figures show a good correspondence between the pressures emitted by each source (real sources) and those estimated using the ICA separation algorithm. This means that the estimation error is low, and therefore, the algorithm or model used is accurate and efficient.

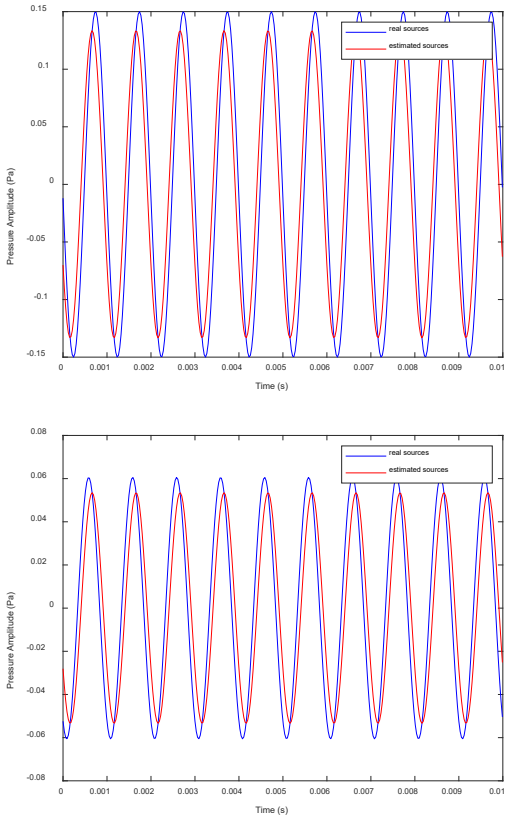

Figure 5. Estimated sources

4.4.2. Sources antiphase

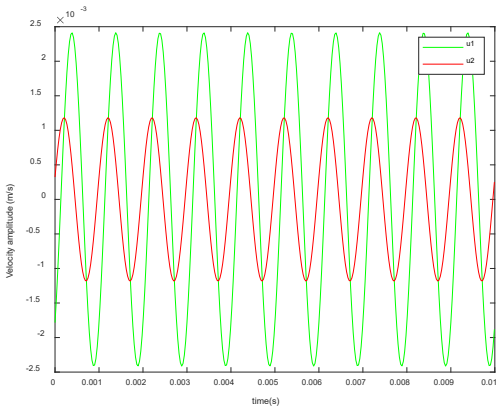

Figure 6. Velocities of sources

We note that in the case of two sources antiphase, the estimated sources present a slight shift compared to the curve of real sources. This is due to the fact that the two sources are vibrating in opposite phase.

The observed differences between in-phase and antiphase dipoles can be explained by their distinct radiation patterns. In-phase dipoles behave similarly to an amplified monopole, producing an almost

isotropic field in the far-field region, which facilitates separation since the sensor signals retain strong amplitude coherence. Conversely, antiphase dipoles generate a figure-eight directivity pattern, leading to directional nulls and phase cancellations. This increases sensitivity to sensor placement and introduces slight waveform shifts in the estimated sources, as seen in the results.

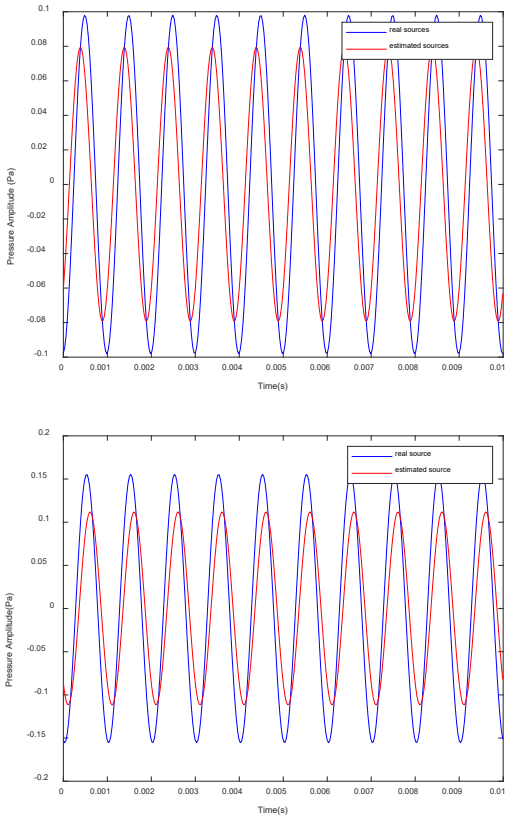

Figure 7. Estimated sources

4.5. Results for acoustic quadrupole

The same measurements are carried out for the case of a quadrupole. Two types of quadrupoles are studied: the longitudinal and lateral quadrupoles.

4.5.1. Longitudinal quadrupole

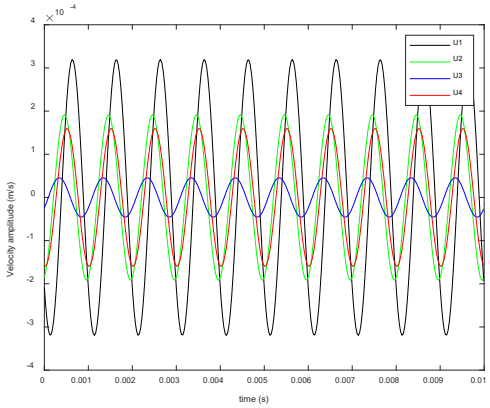

Figure 8. Velocities of each source

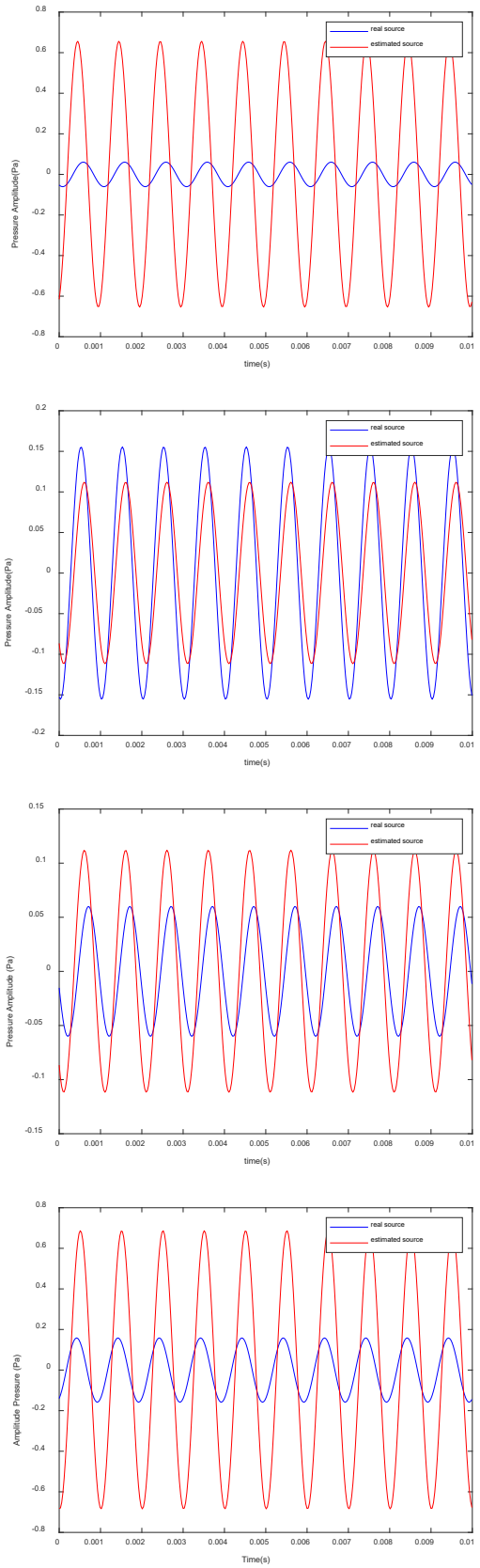

Figure 9. Estimated sources

In the context of sound sources modeled as longitudinal quadrupoles, it is observed that although the estimated sources exhibit similar waveform shapes, temporal patterns, and nearly identical oscillation periods, their amplitudes differ.

This discrepancy arises from the nature of the ICA (Independent Component Analysis) algorithm, which estimates sources from a mixing matrix only up to a scalar factor. Consequently, the amplitude of the reconstructed signals may vary, even when their structural characteristics are preserved.

4.5.2. Lateral quadrupole

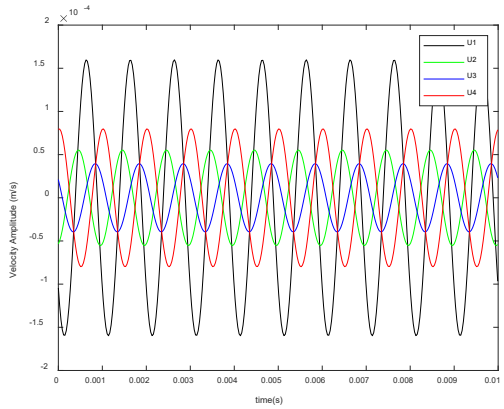

Figure 10. Velocities of each source

Similar to the case of longitudinal quadrupole sources, a comparable pattern is observed with lateral quadrupole configurations. While the reconstructed sources successfully preserve the waveform morphology and exhibit nearly identical oscillation frequencies as the original sources, a noticeable discrepancy in amplitude remains. This divergence is primarily attributed to the inherent limitations of the ICA algorithm, which estimates source signals from a mixing matrix only up to an arbitrary scaling factor.

As the number of sources increases, the complexity of the estimation process grows accordingly. Nevertheless, the algorithm consistently demonstrates the ability to recover the temporal structure and frequency content of the pressure signals emitted by the sources.

For quadrupoles, the longitudinal configuration concentrates energy along the axis of alignment, creating lobes with alternating polarity, while the lateral configuration distributes energy more evenly in orthogonal directions. These spatial characteristics explain why ICA preserves waveform morphology but exhibits amplitude scaling ambiguities: the mixing matrix reflects geometric attenuation and phase differences inherent to multipole radiation. Such behaviors are consistent with classical acoustic theory and highlight the importance of sensor geometry in blind source separation.

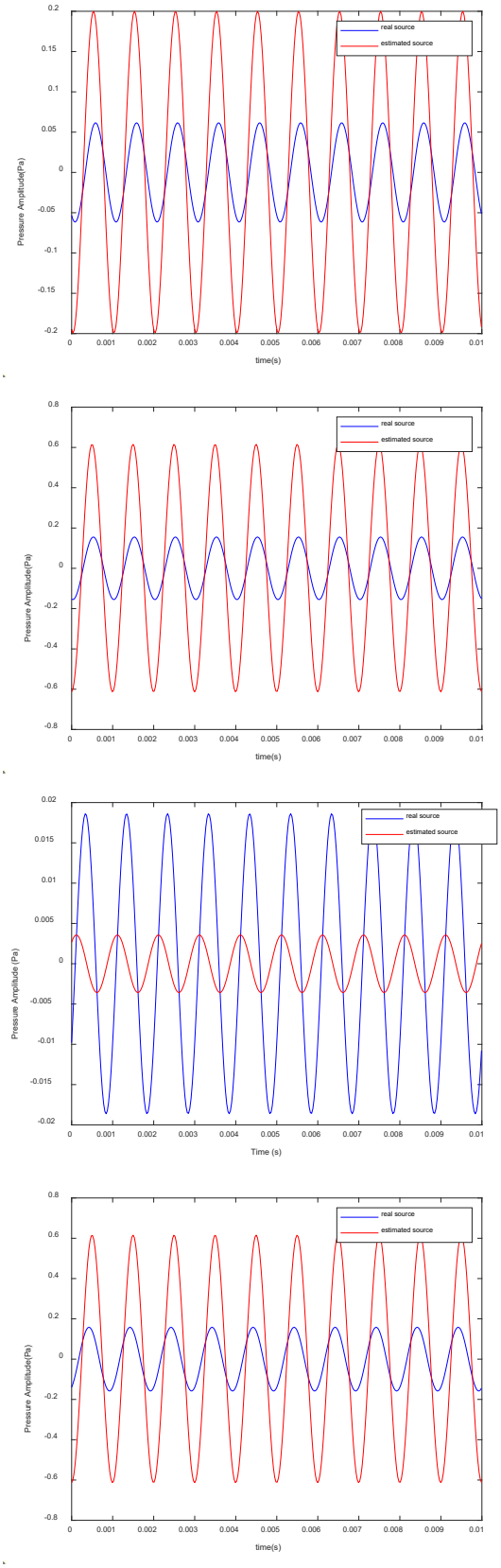

Figure11. Estimated sources

4.6. Evaluation metrics

In the field of signal processing, it is essential to have objective indicators to quantify the quality of the estimated signals compared to the reference

signals. Among the most used metrics are the correlation coefficient |ρ|, the Scale-Invariant Signal-to-Distortion Ratio (SI-SDR), and the Normalized Mean Square Error (NMSE). These measures offer complementary perspectives:

- |ρ| evaluates the statistical similarity between two signals, indicating their correlation in amplitude and shape.

$$|\rho| = \frac{\sum_n s_{original}(n)\, s_{estimated}}{\sqrt{\sum_n s^2{}_{original}(n)} \cdot \sqrt{\sum_n s^2{}_{estimated}(n)}} \quad (31)$$

- SI-SDR measures the distortion introduced by processing, while being insensitive to scale variations, making it particularly suitable for signal separation or enhancement systems.

$$SI-SDR = 10\log\left(\frac{\left\|\alpha s_{original}\right\|^2}{\left\|\alpha s_{original} - s_{estimated}\right\|^2}\right) \; avec \; \alpha = \frac{\left\langle s_{estimated}, s_{original}\right\rangle}{\left\|s_{original}\right\|^2} \quad (32)$$

- The NMSE quantifies the normalized mean square error, providing a direct indication of the accuracy of the estimate.

$$NMSE = \frac{\sum_n \left(s_{original}(n) - s_{estimated}(n)\right)^2}{\sum_n \left(s_{original}(n)\right)^2} \quad (33)$$

We have tested these metrics on the case of antiphase dipole and longitudinal quadripole we obtain the following results:

Scenario	Scenario	Mean ρ	Mean SI-SDR	Mean NMSE
Dipole anti-phase	Dipole anti-phase	0.920	+7.40	-5.12
Quadrupole longitudinal	Quadrupole longitudinal	0.936	+8.45	-11.98

ICA achieves excellent separation for these studied cases in realistic scenarios:

5. CONCLUSIONS

This study has explored the application of Independent Component Analysis (ICA) for the separation and identification of acoustic sources, particularly in the context of vibrating systems modeled as monopoles, dipoles, and quadrupoles. Through a series of simulations involving both lateral and longitudinal quadrupole configurations, it was demonstrated that ICA is capable of accurately reconstructing the temporal structure and frequency content of the original sources, despite inherent limitations such as amplitude scaling ambiguities. The results confirm that ICA remains a robust and effective blind source separation technique, especially when the independence criterion is appropriately chosen. As the number of sources increases, the complexity of the separation task grows; however, the algorithm continues to preserve essential features of the pressure signals. These findings reinforce the potential of ICA-based methods for acoustic source analysis and contribute to the development of reliable diagnostic tools in mechanical and industrial environments.

However, this work is based **on** idealized conditions**:** synthetic signals, noise-free environments, and simplified geometries. These assumptions limit the direct applicability of the findings to real-world scenarios. Future research will address these limitations by incorporating realistic sensor noise**,** parameter uncertainties, and reverberation effects**.** We also plan to validate the approach on experimental data and extend the methodology to overdetermined cases (more sensors than sources) and to more complex source distributions**.** Such developments will enable a comprehensive assessment of ICA's robustness and its potential for industrial diagnostics and acoustic imaging applications**.**

REFERENCES

[1] Mansouri, S., Noroozinejad, Farsangi, E., Adequacy of equivalent static analysis method employing Caltrans, AASHTO, and ATC-32 Provisions in response estimation of vibration-controlled bridges, *ASCE's Journal of Structural Design and Construction Practice*, Vol. 29, Issue 1, 2024. (ASCE), https://doi.org/10.1061/ PPSCFX.SCENG-1340

[2] Mansouri, S., Kontoni, D., P., Pouraminian, M., The effects of selection and scaling procedures of earthquake records on seismic response dispersion of structures and recommendations toward seismic upgrading of codes, *Asian Journal of Civil Engineering*, Vol. 25, pp. 81–96, 2024, (Springer), https://doi.org/10.1007/s42107-023-00758-3

[3] Mansouri, S., Kontoni, D., P., Pouraminian, M., The effects of the duration, intensity, and magnitude of far-fault earthquakes on the seismic response of RC bridges retrofitted with seismic bearings, *Advances in Bridge Engineering*, Vol. 3, Article number: 19, 2022, (Springer), https://doi.org/10.1186/s43251 022 00069 8

[4] Gerges, S., Sehrndt, G., Parthey, W., Noise sources*, In the book, Occupational Exposure to Noise*, Chapter 5, 2001.

[5] Woodhouse, J., *Euphonics - The science of musical instrument*, chapter 7, 14 august 2021.

[6] Russell, D., Acoustics and Vibration Animations, *Graduate Program in Acoustics*, Penn State, August 25, 1998.

[7] Russell, D., Titlow, J. P., and Bemmen, Y., Acoustic monopoles, dipoles, and quadrupoles: An experiment revisited, *Am. J. Phys.* 67 (8), August 1999.
[8] Ochmann, M., Exact analytical solutions for sound radiation from a moving monopole above an impedance plane, *The Journal of the Acoustical Society of America*, 133(4), 1911–1921, (2013). https://doi.org/10.1121/1.4794389)
[9] Kayser, B., Dragna, D., & Blanc-Benon, P., Heuristic solution for the acoustic radiation of a moving monopole in an inhomogeneous and moving atmosphere, *Application to aircraft noise. Acta Acustica*, 8, 62, (2024), https://doi.org/10.1051/aacus/2024048
[10] Moruzzi, M. C., Cinefra, M., & Bagassi, S., Analysis of an acoustic monopole source in a closed cavity via CUF finite elements, *Aerotecnica Missili & Spazio*, 9 August 2022. https://doi.org/10.1007/s42496-022-00129-2
[11] Duan, W., & Kirby, R., The sound power output of a monopole source in a cylindrical pipe containing area discontinuities, *Acoustics — 2012*, 23 April 2012 (HAL preprint).
[12] Zhan, X., Chen, S., Fang, D., & Shi, T., Low-frequency noise reduction mechanism and acoustic characteristics of the dipole surface source structure, *Journal of Vibration Engineering & Technologies*, 2024, https://doi.org/10.1007/s42417-024-01522-w.
[13] Eastland, G. C., Curry, P. J., & Tolliver, L. C. Investigations into acoustic dipole helical wave generation, *The Journal of the Acoustical Society of America,* 152(5), 2929–2933, (2022). https://doi.org/10.1121/10.0015137.
[14] Martischang, J.-P., Roux, A., & Baudoin, M., Acoustic dipole surfing on its own acoustic field, *Toward acoustic quantum analogues*, arXiv, July 2023, https://doi.org/10.48550/arXiv.2307.06642.
[15] Kopyev, V. F., Chernyshev, S. A., Faranosov, G. A., & Korobov, A. A., Validation of a quadrupole model of sound radiation of a turbulent jet based on multi-microphone acoustic measurements, *Acoustical Physics*, 70(5), 710–724, (2024), https://doi.org/10.1134/S1063771024602814.
[16] Brentner, K. S., The exact calculation of quadrupole sources for some incompressible flows (NASA Tech. Mem. 100623). 1988, National Aeronautics and Space Administration.
[17] Kojima, Y., Skene, C. S., Yeh, C.-A., Taira, K., & Kameda, M. On the origin of quadrupole sound from a two-dimensional aerofoil trailing edge, *Journal of Fluid Mechanics*, 958, A3, 2023, https://doi.org/10.1017/jfm.2023.37.
[18] Hérault. J., Jutten, C. et Ans, B., Détection de grandeurs primitives dans un message composite par une architecture de calcul neuromimétique en apprentissage non supervisé, *In GRETSI*, pages 1017–1022, Nice, France, Mai 1985.
[19] Jutten, C., & Hérault, J., Blind separation of sources, Part I: An adaptive algorithm based on neuromimetic architecture*,* 1991, *Signal Processing*, 24(1), 1–10. https://doi.org/10.1016/0165-1684(91)90079-X
[20] Bell, A. J., & Sejnowski, T. J., An information-maximization approach to blind separation and blind deconvolution, *Neural Computation*, 7(6), 1129–1159, 1995, https://doi.org/10.1162/neco.1995.7.6.1129
[21] Hyvärinen, A., & Oja, E., A fast fixed-point algorithm for independent component analysis*, Neural Computation*, 9(7), pp. 1483–1492, (1997). https://doi.org/10.1162/neco.1997.9.7.1483.
[22] Hyvärinen, A., Karhunen, J., & Oja, E., *Independent Component Analysis*, John Wiley & Sons. (2001). https://doi.org/10.1002/0471221317
[23] Comon, P., & Jutten, C. (Eds.), *Handbook of Blind Source Separation: Independent Component Analysis and Applications*. Academic Press (2010). https://doi.org/10.1016/B978-0-12-374726-6.00001-9
[24] Mansour, A., Kawamoto, M., & Ohnishi, N., A survey of the performance indexes of ICA algorithms, *In Proceedings of the International Conference on Modelling, Identification and Control*, (MIC '02). (2002).
[25] Sawada, H., Araki, S., & Makino, S., Underdetermined convolutive blind source separation via frequency-bin-wise clustering and permutation alignment, (2010), https://doi.org/10.1109/TASL.2010.2093230.
[26] Li., D., Wu, M., Yu., L., Han, J. and Zhang, H., Single-channel blind source separation of underwater acoustic signals using improved NMF and FastICA, *Frontiers in Marine Science Journal,* 16 January 2023.
[27] Al-Qaisi, A., Blind Source Separation of Mixed Noisy Audio Signals Using an Improved FastICA, *Journal of Applied Science,* 15 (9): 1158-1166, 2015
[28] Taktak, M., Tounsi, D., Akrout, A., Abbès, M.S. and Haddar, M., One stage spur gear transmission crankcase diagnosis using the independent components method, *Int. J. Vehicle Noise and Vibration*, Vol. 8, No. 4, 2012.
[29] Akrout, A., Tounsi, D., Taktak, M., Abbes, M.S., Haddar, M., Inverse Method For A One-Stage Spur Gear Diagnosis, *Journal Of Theoretical And Applied Mechanics*, 53, 3, pp. 617-628, Warsaw, 2015.
[30] Wu., X, Boustany, R., Bouley, S., Minck, O., Denayer, H., Antoni, J., Gryllias, K., Enhancing blind separation of incoherent sources in acoustic imaging with deep learning*, J. Acoust. Soc. Am.,* 158, 759–775, (2025).
[31] Møller Juhl, P., *Radiation of sound,* Institute of Technology and Innovation, University of Southern Denmark, (2011).
[32] Pelat, A., *Elementary Acoustic Fields,* Engineering School, France, 2020, ffhal-02538652ff
[33] Russel, D., *On the sound field radiated by a tuning fork*, American Journal of Physics, 68(12),1139–1145, 2000.
[34] Comon, P., Independent component analysis, A new concept?*, Signal processing*, 24 August 1992, France, pp. 287-314, 1994.
[35] Hyvärinen, A., & Oja, E., *Independent Component Analysis: Algorithms and Applications*. Neural Networks, *13*(4–5), 411–430, (2000), https://doi.org/10.1016/S0893-6080(00)00026-5.
[36] Chen, S.S, Donoho, D.L., and Saunders, M.A., Atomic decomposition by basis pursuit, Journal on Scientific Computing, vol 20, ISS.1, 1998.
[37] Jones, M.C. and Sibson, R., What is projection pursuit?, *J. of the Royal Statistical Society, Ser. A*, 150, pp. 1–36. 1987.